

A Study of the Near-Ultraviolet Spectrum of Vega

Alejandro García-Gil

*Instituto de Astrofísica de Canarias, c/Vía Láctea s/n, E-38200, La Laguna, Tenerife,
Spain*

agg@ll.iac.es

Ramón J. García López

*Instituto de Astrofísica de Canarias, c/Vía Láctea s/n, E-38200, La Laguna, Tenerife,
Spain*

*Departamento de Astrofísica, Universidad de La Laguna, Avenida Astrofísico Francisco
Sánchez s/n, E-38206, La Laguna, Tenerife, Spain*

rgl@ll.iac.es

Carlos Allende Prieto

*McDonald Observatory and Department of Astronomy, The University of Texas, Austin,
TX 78712-1083, USA*

callende@hebe.as.utexas.edu

and

Ivan Hubeny

AURA/NOAO, Tucson, AZ 85726-6731, USA

hubeny@tlusty.gsfc.nasa.gov

ABSTRACT

UV, optical, and near-IR spectra of Vega have been combined to test our understanding of stellar atmospheric opacities, and to examine the possibility of constraining chemical abundances from low-resolution UV fluxes. We have carried out a detailed analysis assuming Local Thermodynamic Equilibrium (LTE) to identify the most important contributors to the UV continuous opacity: H, H⁻, C I, and Si II. Our analysis also assumes that Vega is spherically symmetric and its atmosphere is well described with the plane parallel approximation.

Comparing observations and computed fluxes we have been able to discriminate between two different flux scales that have been proposed, the IUE-INES and the HST scales, favoring the latter. The effective temperature and angular diameter derived from the analysis of observed optical and near-UV spectra are in very good agreement with previous determinations based on different techniques. The silicon abundance is poorly constrained by the UV observations of the continuum and strong lines, but the situation is more favorable for carbon and the abundances inferred from the UV continuum and optical absorption lines are in good agreement. Some spectral intervals in the UV spectrum of Vega that the calculations do not reproduce well are likely affected by deviations from LTE, but we conclude that our understanding of UV atmospheric opacities is fairly complete for early A-type stars.

Subject headings: stars: atmospheres — stars: fundamental parameters — stars: abundances — stars: individual (Vega) — techniques: spectrophotometry — ultraviolet: general

1. Introduction

Understanding the formation of the UV spectrum of individual stars is essential in order to quantitatively determine stellar abundances for a number of chemical elements that only produce measurable features in the UV domain such as B, Be, or the neutron capture elements Pb and Ge. A proper understanding of the spectra of individual stars is also crucial to interpret integrated light from galaxies and other stellar systems. The UV radiation field, besides affecting directly the abundances obtained from UV lines, has an important effect on the construction of atmospheric models through the energy balance. Theoretical atmospheric structures computed under the assumptions of radiative equilibrium and local thermodynamical equilibrium are routinely employed in the analysis of spectra from astronomical objects. Consequently, an error in the UV opacities translates into wrongly derived physical properties, namely, chemical composition and atmospheric parameters for individual stars, or ages for galaxies.

A possible UV opacity source missing from the calculations has been proposed to explain an early reported failure to match the observed solar UV spectrum. It has been suggested that either line (e.g. Holweger 1970, Vernazza, Avrett & Loeser 1976) or continuum (Bell, Paltoglou & Tripicco 1994, Bell, Balachandran & Bautista 2001) metal absorption could provide that extra opacity. However, several recent studies of UV spectra of other stars suggest that there is a reasonable agreement between theoretical models (Kurucz 1992) and

observations (e.g. Allende Prieto & Lambert 2000, Fitzpatrick & Massa 1999, Peterson et al. 2001). The analysis of the solar spectrum by Bell, Balachandran, & Bautista (2001) concluded that even when using the most recent calculations of line and continuum opacities, classical model atmospheres predict too much UV flux. Nonetheless, this result has been challenged by independent calculations by Allende Prieto, Hubeny & Lambert (2003), who found that LTE modeling can reproduce closely the observed solar flux at wavelengths longer than about 2600 Å, and uncertainties in the atomic line data fully account for the differences between computed and observed fluxes. High quality observations of stars with different atmospheric parameters than the Sun present a promising way to solve the controversy.

There is a second controversy that affects the absolute flux scale of UV observations. The most recent calibration of the *International Ultraviolet Explorer* (IUE) archive has been dubbed INES (*IUE Newly Extracted Spectra*), and will be discussed more deeply in the following section. IUE obtained the largest available collection of astronomical UV spectra. There are at least two more calibrations of IUE, both taking spectra to the HST flux scale, which is 7.2 % lower than the INES scale (González-Riestra, Cassatella, & Wamsteker 2001). These calibrations will be explained in Sect. 2. Clarifying which flux scale should be adopted is a must to properly interpret observations.

In this paper we deal with Vega (α Lyr, HD 172167, A0V). This star is not straightforward to model, because it has a dust and gas disk (Walgate 1983; Wilner et al. 2002) which produces an IR flux excess; it is a fast rotator seen pole-on (Gulliver et al. 1994); and it is possibly variable (Vasil’Yev et al. 1989). Moreover, it has a peculiar abundance pattern, similar to that of λ Boo stars (Ilijić et al. 1998), that is, with a relative underabundance of Fe-like elements with respect to the Sun, but solar proportions of C, N, O, and S. Despite these difficulties, Vega is one of the few dwarf stars that can be used to test detailed calculations of UV irradiances: both precise UV spectrophotometry and independent measurements of its angular diameter are available. Visible high resolution and high signal-to-noise ratio (S/N) spectra of Vega are also readily obtained from the ground. Besides, the disk is expected to make no detectable contribution to the star’s visible and UV spectrum, and it has been found that the influence of fast rotation is only important for the shape of spectral lines, with a small effect on the continuum limited to the spectral region in the vicinity of the Balmer jump (Gulliver et al. 1994).

Our analysis puts to the test calculations of UV irradiances based on classical (Kurucz 1992) model atmospheres and modern line and continuous opacities. In addition to UV spectrophotometry of the star, we also use optical spectrophotometry and high-dispersion optical spectra to constrain the chemical abundances and narrow down the ranges of the involved model parameters. In § 2, we present a description of the observations employed.

In § 3, we describe the analysis carried out and the results obtained, whose consequences are discussed in § 4.

2. Description of the observations

We have considered three versions of the average low-dispersion IUE spectrum of Vega:

- INES; this is not a calibration of IUE data processed with NEWSIPS (*New Spectroscopic Image Processing System*; see Garhart et al. 1997), but a new full processing of the raw data, improving the spectrum extraction to diminish the error sources present in NEWSIPS (improving the noise model, the extraction method, the homogenization of the wavelength scale, and the flagging of the absolute calibrated extracted spectra). The relative fluxes were calibrated using a pure H (DA) white dwarf, G191B2B, whose virtually featureless spectrum is relatively simple to model. The absolute flux scale relies on that of the UV satellite OAO-2 (González-Riestra, Cassatella, & Wamsteker 2001).
- Bohlin’s calibration (Bohlin 1996), obtained from the CALSPEC Web page ¹; 8 standard stars (4 DA’s among them) are used to calibrate FOS (*Faint Object Spectrograph*) observations, formerly onboard HST. By comparing their FOS and IUE fluxes, a correction factor is determined, which is applied to each wavelength of a IUESIPS (the earlier version of NEWSIPS) spectrum of Vega to place the data in the HST flux scale. This set of standard spectra has been updated by new STIS and NICMOS observations (both onboard HST; Bohlin, Dickinson, & Calzetti 2001)². The zero level of the flux scale is tied to the average over the V band for Vega as measured by Hayes (1985).
- Massa & Fitzpatrick’s calibration (Massa & Fitzpatrick 2000, hereafter M&F); it takes into account the systematic errors in NEWSIPS spectra with the observation time and the temperature of the amplifying camera (THDA), and applies a correction factor to place the data into the HST scale.

The three versions above are based on low-dispersion large-aperture IUE spectra, but the particular individual spectra considered in the average, and some parts of the processing

¹<http://kahuna.stsci.edu/instruments/observatory/cdbs/calspec.html>

²The spectrum we use in this article is not the one obtained with STIS and recently published (Bohlin & Gilliland 2004), but the earlier one, since this one was not yet published at the time this study was carried out

(chiefly, the flux calibration) differ among them. These spectra have a large spectral coverage with a resolution of $\sim 6 \text{ \AA}$. We combined several IUE spectra from the INES and MAST³ servers to produce the INES and M&F versions, respectively. The list of individual spectra is provided in Table 1. Before combining the MAST-IUE spectra to produce the M&F version, the fluxes were processed with the software kindly provided by these authors. Bohlin’s spectrum was directly obtained from the STScI web pages, as provided by R. Bohlin⁴.

As we can see in Fig. 1, Bohlin’s and M&F fluxes (which share the same flux scale) are $\sim 10\%$ higher than the INES fluxes for Vega. This is higher, but roughly consistent within the error bars with the global differences reported by González-Riestra, Cassatella, & Wamsteker (2001) between FOS and IUE spectra for the INES reference star G191B2B. However, they noticed an almost linear reduction from a difference of $\sim 7\%$ at 1500 \AA to $\sim 6\%$ at 3000 \AA , while we find larger differences for Vega in the ranges 1500 to 1700 \AA and 2000 to 2500 \AA . Fig. 1 reveals that the M&F flux is higher than Bohlin’s at ~ 1800 and $\sim 2000 \text{ \AA}$. The feature in the M&F version at $\sim 2000 \text{ \AA}$ coincides with the border between the short and long-wavelength cameras, where the uncertainty in the flux is higher.

We have also compared our calculations with high-resolution IUE spectra. These spectra have a large spectral coverage with a resolution $\sim 0.2 \text{ \AA}$. Table 1 lists the high-resolution spectra considered, which were corrected in absolute flux to put them into the HST scale and then averaged to obtain the final one.

We also compared Bohlin’s and INES fluxes for the eight primary standard stars on which Bohlin’s fluxes are based (G191B2B, GD153, GD71, HZ43, HZ44, BD +28 4211, BD +33 2642, and BD +75 325). We used all the IUE spectra available for these stars from the INES database, selecting only those pixels labeled with good quality and with flux errors lower than 20% . Bohlin’s flux is again higher than the INES one at all wavelengths and for all the stars, with the exception of the SWP spectrum of BD +75 325. The mean relative difference in flux for the other seven stars is $(F_{Bohlin} - F_{INES})/F_{INES} = 0.066 \pm 0.013$, which is again consistent with the global differences reported by González-Riestra, Cassatella, & Wamsteker (2001). When studying the wavelength dependence, an increment of the difference is seen at $\sim 2000 \text{ \AA}$ and from 2200 to 2500 \AA , where the difference is over 8% , while in the other regions it is $5\text{-}7\%$, quite consistent with the larger differences observed in Vega’s case between 2000 and 2500 \AA .

³Multi-mission Archive at Space Telescope

⁴URL is <ftp://ftp.stsci.edu/cdbs/cdbs2/calspec/>

Visible spectrophotometry provides additional information that cannot be neglected. We consider the spectrum compiled by Hayes (1985) by combining six different sources of ground-based measurements. This spectrum has a flux uncertainty of just about 1-2% in the optical and covers a wavelength range from 3300 to 10500 Å. The flux is tabulated in steps of 25 Å. This is both the bandwidth and step sizes reported by Terez (1982) and Arkharov & Terez (1982), who measured Vega’s flux in the entire region critically evaluated by Hayes. The other sources considered by Hayes provide fluxes measured over smaller spectral ranges with bandpasses from 10 to 100 Å, and approximate corrections for the bandwidth. Based on this information, it seems therefore appropriate to compare these data to calculated fluxes smoothed to a resolution of at least 50 Å.

In addition to the basic atmospheric parameters: effective temperature, surface gravity, and overall metallicity, the abundances of particular elements, whose ratio to iron may differ from solar, may affect the spectral energy distribution in the UV. Initial estimates of those abundances are necessary to perform a meaningful comparison of computed and observed UV fluxes. The analysis of optical spectral lines provides abundances for the most relevant elements.

We have used two different spectra, with different resolving power, obtained by our group at McDonald Observatory (Mount Locke, Texas), acquired with the *2dcoudé* cross-dispersed echelle spectrograph (Tull et al. 1995) coupled to the Harlan J. Smith 2.7m Telescope. The first spectrum is part of the S⁴N survey of nearby stars (Allende Prieto et al. 2004) and is the average of observations secured in May 1 and 2, 2001. It has a resolving power ($R \equiv \frac{\lambda}{\delta\lambda}$) of $\sim 5 \times 10^4$, covering in full the optical range, extending into the near IR. As the spectrograph provides full coverage only from about 3600 Å to ~ 5100 Å in a single exposure for this resolution, with increasingly larger gaps between redder orders, two overlapping settings were used to circumvent the problem. The second spectrum was obtained at the focal station F1, and has $R \sim 173000$, covers the range from ~ 4400 to ~ 7600 Å with some small gaps, and was obtained in June 9–12, 2000. The spectral coverage is much smaller at F1, and 10 tilts of the grating/prisms were needed to achieve the final coverage. The CCD registered pieces of ~ 16 adjacent orders.

For both the high- and intermediate-resolution spectra, the detector was TK3, a thinned 2048×2048 Tektronix CCD with 24 μm pixels, and we used grating E2, a 53.67 gr mm^{-1} R2 echelle from Milton Roy Co. For the spectrum with $R \sim 6 \times 10^4$, we used slit #4, which has a central width of 511 μm (or approx. 1.2 arcsec on the sky). For the spectrum with $R \sim 173000$, we used slit #2, which has a central width of 145 μm , and partially

masked the collimator. A careful data reduction was applied to both spectra, using IRAF⁵, which consisted of overscan (bias) and scattered-light subtraction; flatfielding; extraction of one-dimensional spectra; wavelength calibration; and continuum normalization.

3. Analysis

3.1. Chemical species affecting the visible and the UV continuum

A few particular elements may contribute significant opacity in the UV. Iron is known to dominate line absorption virtually for all spectral types. Continuous absorption from other metals may also be significant or even dominant. The main contributors to the UV continuous opacity change with the spectral type and, therefore, it is important to evaluate which metals are relevant and provide reasonable estimates of their abundances to calculate realistic UV fluxes. The ability of an ion to contribute bound-free opacity depends on its atomic structure and its abundance. As a preliminary step, ion abundances for the 30 first elements in the first three states of ionization were computed for a star like Vega, using the model parameters preferred by Castelli & Kurucz (1994; an effective temperature $T_{\text{eff}} = 9550$ K and gravity $\log g = 3.95$) using Saha and Boltzmann equations. At this point we simply assumed solar photospheric abundances (Anders & Grevesse 1989).

Next, we computed synthetic visible and near-UV spectra including continuous opacity produced by only H (including bound-bound H opacity, i.e. hydrogen lines, as part of continuous opacity) and each of the most abundant ions in Vega. The calculations were carried out with the program SYNPLLOT, a wrapper of SYNSPEC (Hubeny & Lanz 2000) for IDL. Bound-free opacities were obtained from TOPBASE (Cunto et al. 1993) and smoothed to dilute resonances whose exact frequencies are not accurately known (Allende Prieto et al. 2003). We studied all the ions with abundances relative to H larger than 10^{-6} : He I, C I, C II, N I, N II, O I, O II, Na II, Mg II, Al II, Si II, S II, Ca II, Fe II and Ni II. A contribution could be missed if it corresponds to an ion with a low abundance but an unusually high photoionization cross section, but we believe our list is complete. For these calculations, the atmospheric parameters of Castelli & Kurucz (1994) were used as well as solar abundances for each element, except for Fe, for which it was adopted $[\text{Fe}/\text{H}] = -0.38$, to be consistent with the model atmosphere: $[\text{M}/\text{H}] = -0.5$ (see the discussion in Fitzpatrick & Massa 1999). By comparing the spectra derived including continuous opacity due to H plus any given ion

⁵IRAF is distributed by the National Optical Astronomy Observatories, which are operated by the Association of Universities for Research in Astronomy, Inc., under cooperative agreement with the National Science Foundation

to that obtained including only neutral H continuous opacity, we deduce the relevance of each ion’s continuous opacity to the observed fluxes. This is illustrated in Fig. 2 for the most important contributors. Hydrogen bound-free and line absorption dominate the opacity blueward of L_α , shaping the near-UV and optical spectrum of Vega. At wavelengths longer than about 1500 Å, neutral hydrogen and the H^- ion dominate the total bound-free opacity. Si and C contribute significantly to the continuous opacity between 1200 and 1450 Å. He I would also appear in the figure below 1400 Å with a maximum of $\sim 1.5\%$, but it has not been included for clarity.

Fig. 3 shows the continuum and line absorption due to each ion. Fe I lines swamp the UV spectrum of solar-like stars. At the temperatures in Vega’s photosphere, iron is almost completely ionized ($N_{\text{FeI}}/N_{\text{FeII}} \sim 10^{-4}$), and the atomic line absorption is mainly produced by Fe II (around half the total absorption of lines and most of the absorption due to Fe lines). Molecules are virtually inexistent at these warm temperatures. We considered different sources for the atomic line data, finding that a linelist based on data compiled by Kurucz and distributed with SYNPLLOT provided the best results. The agreement with the observations was only marginally improved when updating Stark line damping parameters extracted from VALD⁶ (Kupka et al. 1999). All the fluxes shown in Fig. 3 include a contribution to the total opacity by incoherent electron scattering. Although Thomson scattering is wavelength independent, the vertical structure of the atmosphere makes its role maximum at about 1300 Å, where it effectively reduces the emerging flux by about 4 %, and over 1 % for $\lambda < 2000$ Å.

In conclusion, to model the UV spectrum of a star like Vega it is necessary to account for H, C, Si, and Fe opacities in as much detail as possible.

3.2. Estimation of T_{eff} and θ by using visible and near-UV regions

Allende Prieto & Lambert (1999) estimated a set of fundamental parameters for a large sample of nearby stars, using Hipparcos parallaxes to accurately constrain their positions in the color-magnitude diagram. Comparison with evolutionary calculations by Bertelli et al. (1994) allowed them to provide masses, radii, gravities and effective temperatures for 17,219 stars. Their estimate for Vega provides: $\log g = 3.98 \pm 0.02$. Given the limited effect of gravity on the UV spectrum, we will adopt this value and attempt to determine the effective temperature and angular diameter from the observations in the optical and near-infrared. This can be achieved by comparing the computed emitted flux from Kurucz model

⁶Van der Waals parameters are similar, so we have maintained them

grids (which have $\log g$ and T_{eff} as the independent parameters), transformed to computed received flux by using the angular diameter, to the observed flux. In these regions, metal absorption is modest, which allows us to study these two parameters fairly independent of the details of the chemical composition.

We minimized the sum of χ^2 statistics between observed and computed spectra in three wavelength regions weighted according to the approximate uncertainty in the observed fluxes inferred from Bohlin’s analysis in the UV and Hayes’ in the visible range, respectively (4% between 1600 and 2150 Å and between 2200 and 3000 Å, and 2% between 4150 and 8480 Å, excluding Balmer lines). We used the Nelder-Mead simplex algorithm (Nelder & Mead 1965) for the minimization. Using SYNSPEC, we computed a grid of fluxes based on interpolated Kurucz’s model atmospheres (Kurucz 1992) with T_{eff} running between 9350 and 9650 K. As the model atmospheres are available in steps of 250 K, we linearly interpolated all the relevant quantities as a function of the optical depth. We matched selected spectral regions, excluding the segments where special difficulties exist. In particular, the spectrum in the vicinity of the Balmer jump (3000–4150 Å) was discarded because Hayes advises about significant errors in this region and the effect of fast rotation is important (Gulliver et al. 1994). At this stage, a solar He abundance was used and the metal abundances are from Qiu et al. (2001), including $[\text{Fe}/\text{H}] = -0.57$ dex, which was adopted as the metallicity for the model atmosphere $[\text{M}/\text{H}] = -0.7$ dex, using the same conversion factor as Fitzpatrick & Massa (1999). The best-fitting pairs (T_{eff}, θ) and the quality of the fit are displayed in Table 2. The fit is clearly better in the UV using Bohlin’s calibration than using the INES one, so the overall UV flux level is better reproduced with synthetic spectra when the observed spectrum is in Bohlin’s scale. Fig. 4 confronts the observed flux (using Bohlin’s calibration in the top panel and the INES calibration in the bottom panel) and the computed flux that best matches it. In that figure, the computed flux is clearly lower than the observed one for $4150 < \lambda < 4500$ Å when using the parameters of the best fit with INES calibration, and it is clearly higher than the observed one for $2200 < \lambda < 3000$ Å. This can be explained when taking into account that INES UV flux is lower than Bohlin’s one, but the same visible observed flux has been used. Then, the computed flux matching the INES calibration is lower than the one matching Bohlin’s UV observed flux, and the same is observed in the visible next to the UV region. Such effect is the result of diminishing T_{eff} and increasing θ to match the INES scale.

A comparison between these parameters for Vega and those taken from the literature is made in Table 3. The selected literature values do not include analyses of UV spectra from IUE. T_{eff} runs the gamut between 9430 and 9660 K and θ between 3.24 and 3.28 mas. These values are consistent with the parameters obtained with Bohlin’s calibration (or with the M&F one, given that both are on the same scale). However, the angular diameter derived

from the analysis of the INES spectrum is significantly higher than the literature values. In addition, there are only two T_{eff} determinations that are consistent with the result we find if the INES calibration is adopted: the extreme value found by Moon & Dworetzky (1985) and that by Ciardi et al. (2001). As the difference in the absolute flux between INES and the other calibrations amounts to more than 10% for Vega, we have derived an average UV spectrum as the mean of Bohlin’s calibration and M&F, not taking into account INES. Using this flux, we have matched again the region between 2200 and 8500 Å (without the zone between 3000 and 4150 Å), obtaining the following result:

$$T_{\text{eff}} = 9620_{-63}^{+49} \text{ K}, \theta = 3.272 \pm 0.03 \text{ mas}$$

where the error bars of our T_{eff} and θ estimations were derived by perturbing the best-fitting parameters until the flux variation exceeded the error bars assigned to the observed spectrum.

The same analysis was carried out using new model atmospheres (Castelli & Kurucz 2003) which were calculated with overshooting turned off (resulting in a steeper rise in temperature with depth in the region where the optical continuum is formed; Castelli, Gratton & Kurucz 1997), and using updated values for the solar elemental abundances and revised opacity distribution functions (ODFNEW). The reason for this new analysis is to check the effect on colors of convective overshoot and the parameters thus obtained were:

$$T_{\text{eff}} = 9575 \text{ K}, \theta = 3.271 \text{ mas},$$

where $\sigma_{2230} = 2.4 \%$ and $\sigma_{4085} = 0.7 \%$. These values provide a slightly better fit, but are nonetheless consistent with those obtained using older model atmospheres and also with most values from the literature.

Fig. 5 compares the observed and calculated fluxes, including the interpolation of calculated fluxes when using ODFNEW model atmospheres with these T_{eff} and θ values and C and Si abundances found in section 3.4. There is a slight flux difference between both synthetic spectra in the region between ~ 1400 and ~ 1900 Å, where the flux using ODFNEW models is higher, except ~ 1560 Å, where there is no change. For instance, the fit is better ~ 1450 Å using ODFNEW models.

Adopting the T_{eff} and $[M/H]$ values from Alonso, Arribas & Martínez-Roger (1994), we searched only for the value of θ leading to the closest match to the observed spectrum in the near-UV and the visible ranges, obtaining again a value of 3.27 mas. Using this angular diameter, the fit to the observed flux is very satisfying in the near-UV and visible spectral ranges, which reinforces the validity of our method. We discuss the UV fluxes below.

A high-resolution spectrum using the interpolation of Kurucz (1992) model atmospheres

with $T_{\text{eff}} = 9620$ K and $\log g = 3.98$, and an angular diameter of 3.27 mas, has been computed and compared with the high-resolution IUE observed spectrum in three 100 Å-wide spectral regions randomly selected between 1550 and 3050 Å, where the effects of rapid rotation and Si and C continuous opacities on the flux are very limited. The standard deviations between the computed and the observed spectra are: 8.5 % in the region centered at 1668 Å, 9.9 % at 2174 Å and 6.9 % at 2550 Å, which, although are higher than the values derived from the low-resolution spectra, reproduce quite well the shape of the high-resolution observations. Fig. 6 compares the computed and the observed fluxes in three 20 Å-wide windows, one in each region.

A preliminary test taking into account the rapid rotation on the emergent flux of spectral lines was also performed. Some of the parameters used ($T_{\text{polar}} = 9595$ K and $i = 6$ degrees) were taken from one of the best fits to the observed flux by Gulliver et al. (1994)⁷, following the procedure used by Pérez Hernández et al. (1999) to compute the flux. This procedure assumes uniform rotation and gravitational potential as a mass point. Using these stellar models with the line Si II $\lambda 4128.07$ Å, the synthetic line becomes deeper and deeper and less and less broad when the rotational velocity decreases, obtaining a good fit with $v_{\text{rot}}(\text{eq}) = 210$ km/s, for which $v \sin i = 22.0$ km/s, consistent with the slow-rotating value. The comparison between the observed line and the computed ones with $v_{\text{rot}}(\text{eq}) = 170, 210$ and 250 km/s is shown in Fig. 7. This effect on the spectral lines will be considered in detail in future articles.

3.3. Estimation of Si and C abundances from the UV continuum

We turn to the main issue we are interested in, the analysis of the UV spectrum. In Section 3.1, we concluded that Si and C were important contributors to the UV continuous opacity for a star like Vega. With the adopted atmospheric parameters (gravity derived from the *Hipparcos* parallax and both T_{eff} and θ from fitting the optical and near-IR flux), we now attempt to constrain the abundances of these elements from the UV flux. We calculated synthetic spectra from 1270 Å to 1380 Å and from 1460 Å to 1550 Å. The region between 1380 and 1460 Å is not considered due to exceptional problems that we discuss below. We considered Si abundances (from Grevesse & Sauval 1998) between $[\text{Si}/\text{H}] = -1.1$ and -0.5 and C abundances between $[\text{C}/\text{H}] = -0.1$ and 0.2, to find C and Si abundances. In Fig. 8,

⁷However, the other parameters used are different. We have used the observed angular diameter (3.27 mas, taken from this paper) and the distance (7.76 pc, obtained from the Hipparcos parallax) to derive the equatorial radius (2.73 R_{solar}), and also the polar radius by using the stellar model. We have also used the mass of a typical A0V star (2.4 M_{solar}) to calculate the surface gravity.

we can see the effect of a change of 0.2 dex in the abundances of C (top panel) and Si (lower panel).

The best fit to the observations is obtained for $[\text{Si}/\text{H}] = -0.90^{+0.57}_{-2.10}$ and $[\text{C}/\text{H}] = 0.03^{+0.34}_{-0.48}$, with $\sigma_{\text{rms}} = 3\%$, approximately the same as the uncertainty of the UV observed spectrum. The error bars take into account the uncertainty in He abundance (assumed ± 0.1 dex), T_{eff} , the observed flux, and Si abundance (C abundance) when computing the error in C abundance (Si abundance), where the first two error sources are the most relevant ones. The values obtained by Qiu et al. (2001) from the analysis of visible lines were $[\text{Si}/\text{H}] = -0.59 \pm 0.06$ and $[\text{C}/\text{H}] = -0.06 \pm 0.13$. The reference solar abundances were adopted from the literature (Grevesse & Sauval 1998) and not derived by us following a similar procedure using the UV solar spectrum.

The large error bars in the UV-based abundances are the result of the relatively weak response of the UV continuum to changes in metal abundances, which is primarily a consequence of the dominant role of hydrogen opacity in such a warm atmosphere. In addition, the existence of several spectral regions where the agreement between observed and computed fluxes is, independently of the adopted abundances, poor, has quite a negative impact on our potential to derive abundances from UV fluxes. Some of the most remarkable discrepancies are associated with deep Si I and C I lines (for instance, at $\sim 1560 \text{ \AA}$ and at $\sim 1660 \text{ \AA}$), likely because departures from LTE, neglected in our calculations, are important. This effect could also affect the C and Si abundances derived from the UV continuum. However, some deep lines of other species (like Fe II) are well reproduced in LTE. A comparison between these C and Si lines in LTE and NLTE with the observed lines is shown in Fig. 9. There is a list of some of the deepest lines in these regions in Table 4. The regions between 1380 and 1460 \AA and between 2000 and 2200 \AA show also a disappointing mismatch between observed and calculated fluxes. The reason for this failure is not clear (although the fit improves when using NLTE, but not enough), and a similar effect appears when using a revised flux of Vega based on STIS spectra (Bohlin, personal communication). These new fluxes agree much better with the computed flux in Balmer lines, thus supporting the exclusion of these lines from our calculations. This flux is lower than the one by Hayes, which would produce a lower T_{eff} and θ to match the computed flux.

3.4. Estimation of abundances by using spectral lines in the visible range

To make a consistent comparison between UV abundances and those derived from spectral lines in the visible region, we have selected a set of clean lines with a log gf uncertainty

$\leq 25\%$ taken from Przybilla (2002)⁸, using their gf values, except for Fe II lines, whose $\log gf$ values were taken from the adopted values in Allende Prieto et al. (2002). We have excluded from consideration He lines, because they are too weak, and the Na I resonance doublet, because of the important departures from LTE in the core of these lines. We have measured the equivalent width (EW) of these lines by integrating the flux over the whole line using the *splot* procedure within IRAF on the visible spectra taken at McDonald Observatory. These EW's were used to derive abundances with MOOG (Snedden 2002). Classical line damping parameters were used, that is, classical natural line broadening was assumed, as well as Unsöld approximation for the Van der Waals broadening, while Stark broadening was neglected. A test about the influence of the Stark broadening using the VALD value on the derived abundances gives similar results as neglecting it.

Tables 5 and 6 show the observed EW of each spectral line (with its uncertainty) and the abundance ($\log N(X/H) + 12$) derived using parameters in the model atmospheres from different references: Qiu et al. (2001, *Qiu* in Tables 5 and 6), Przybilla (2002, *Przybilla* in Tables 6 and 7) and ours (in which we have used a microturbulence of 2 km s^{-1}). Other reasonable values for the microturbulence ($0\text{-}3 \text{ km s}^{-1}$) would have a negligible effect on the mean iron abundance. The mean difference of ~ 0.1 dex between iron abundances derived from Fe I and Fe II lines is perhaps due to the NLTE effects in the formation of the former ones.

Using the abundances obtained from optical spectral lines, we found the mean abundance of each element, shown with its standard deviation in Table 7. In the same table, we show the original abundances found in the literature using the corresponding stellar parameters and, for C and Si, the values that we obtained from the analysis of the UV flux. Besides, solar abundances from Grevesse & Sauval (1998) are shown, written as GS98 in the table. The uncertainties in the line-based abundances due to T_{eff} (9620_{-63}^{+49}K) and to $\log g$ (assumed 3.98 ± 0.1) are in the range $0.01\text{-}0.07$ dex and $0.01\text{-}0.06$ dex, respectively.

We can see from Table 7 that C, N, and O abundances for Vega are similar to those of the Sun, while Mg, Al, Si, Ca, Cr, and Fe abundances are between -0.3 and -0.7 dex compared to the solar ones. This is consistent with previous studies, and suggests that Vega is a mild λ Boo star.

⁸We prefer to revisit the optical abundances for this star because newer, high-quality data is now available, and because that is the only way to guarantee the analysis is fully consistent with our UV study. The reader should, however, keep in mind that our LTE analysis is in some cases more limited than previously published studies such as Przybilla (2002), who studied several species in NLTE

4. Conclusions

We have compiled spectroscopic observations from the literature to globally examine the spectral energy distribution of Vega in the UV, optical and near-IR. We also obtained new high-dispersion optical spectra and derived LTE abundances from atomic lines to further constrain the modeling of the spectral energy distribution.

Different versions of the mean UV spectrum based on IUE data are available, and significant differences ($\sim 7\%$) exist among them. We model Vega’s fluxes as a way to discriminate between the different flux scales. The highest consistency is found adopting the HST flux scale. We identify the most important contributors to the continuum opacity in the UV for Vega. The bound-free opacities of neutral H and the H^- ion play a dominant role above $\sim 1450 \text{ \AA}$. C I is the most important metal contributor below that wavelength, followed by Si II. A solar He abundance has been assumed when calculating the observed spectrum, consistent with some of the previous determinations (e.g. Przybilla 2002), but different to the lower value used by other authors (e.g. in the calculations by Gulliver et al. 1994). This constitutes a non-negligible error source, since a small change in that abundance produces a measurable variation in the abundance of the H species, resulting in a significant change in the continuum opacity or, equivalently, in the computed flux.

The stellar effective temperature (T_{eff}) and the angular diameter (θ) are derived by comparing computed spectra with the observed optical and near UV spectrum above 2200 \AA , where the only important contributors to the continuous opacity are H species, and metal abundances are not very relevant. We obtain $T_{\text{eff}} = 9620_{-63}^{+49} \text{ K}$ and $\theta = 3.272 \pm 0.03 \text{ mas}$. A good agreement between computed and observed spectra is also obtained when using high resolution spectra in the UV, as it is shown for three randomly selected regions. Once the atmospheric parameters were derived, we made use of the UV flux to constrain the C and Si abundances.

The abundance of Si obtained from the UV continuum ($[\text{Si}/\text{H}] = -0.90_{-2.10}^{+0.57}$) is very different from the value we determine from the spectral lines in the optical ($[\text{Si}/\text{H}] = -0.47 \pm 0.14$), but consistent within the large uncertainty of the UV-based value. The abundance of C obtained from the UV continuum ($[\text{C}/\text{H}] = +0.03_{-0.48}^{+0.34}$), however, is in good agreement with the mean value determined from optical lines ($[\text{C}/\text{H}] = -0.13 \pm 0.07$). Departures from LTE are known to affect both C I and Si II lines (Wedemeyer 2001; Stürenburg & Holweger 1990), but are small compared to the uncertainties of our UV-based abundances. We have shown that at least part of the spectral regions of the UV spectrum of Vega that our LTE models cannot reproduce appear to be affected by departures from LTE. In particular, two UV regions with deep C I and Si I lines (~ 1560 and $\sim 1660 \text{ \AA}$) are better reproduced when using NLTE models with C and Si abundances from the UV continuum fit. A further study

of high-dispersion spectra in the UV, departures from LTE in the modeling and the effect of rapid rotation is clearly the next step.

Together with a previous LTE analysis of the UV solar spectrum (Allende Prieto et al. 2003), we arrive at the preliminary conclusion that our understanding of stellar atmospheric opacities in the UV is fairly complete for spectral types A to G. Departures from LTE may contribute somewhat for the solar case, but are expected to be more important for a star like Vega (see, e.g., Hubeny 1991; Hauschildt et al. 1999). In the case of Vega, the distortion from spherical symmetry induced by rapid rotation must be accounted for, in order to disentangle such effect from departures from LTE and other approximations adopted.

REFERENCES

- Allende Prieto, C., & Lambert, D. L. 1999, *A&A*, 352, 555
- Allende Prieto, C., & Lambert, D. L. 2000, *AJ*, 119, 2445
- Allende Prieto, C., Asplund, M., García López, R. J., & Lambert, D. L. 2002, *ApJ*, 567, 544
- Allende Prieto, C., Hubeny, I., & Lambert, D. L. 2003, 591, 1192
- Allende Prieto, C., Barklem, P. S., Lambert, D. L., & Cunha, K. 2004, *A&A*, 420, 183
- Alonso, A., Arribas, S., & Martínez-Roger, C. 1994, *A&A*, 282, 684
- Anders, E., & Grevesse, N. 1989, *Geochimica et Cosmochimica Acta*, 53, 197
- Arkharov, A. A., & Terezh, È. I. 1982, preprint
- Bell, R. A., Paltoglou, G., & Tripicco, M. J. 1994, *MNRAS*, 268, 771
- Bell, R. A., Balachandran, S. C., & Bautista, M. 2001, *ApJL*, 546, L65
- Bertelli, G., Bressan, A., Chiosi, C., Fagotto, F., & Nasi, E. 1994, *A&AS*, 106, 275
- Bohlin, R. C. 1996, *AJ*, 111, 1743
- Bohlin, R. C., Dickinson, M. E., & Calzetti, D. 2001, *AJ*, 122, 2118
- Bohlin, R. C., & Gilliland, R. L. 2004, *astro-ph*, 3712
- Castelli, F., Gratton, R. G., & Kurucz, R. L. 1997, *A&A*, 318, 841
- Castelli, F., & Kurucz, R. L., 1994, *A&A*, 281, 817

- Castelli, F., & Kurucz, R. L. 2003, in *Modelling of Stellar Atmospheres*, IAU Symp., 210, ed. N. E. Piskunov, et al., in press
- Ciardi, D. R., van Belle, G. T., Akeson, R. L., Thompson, R. R., Lada, E. A., & Howell, S. B. 2001, *ApJ*, 559, 1147
- Code, A. D., Davis, J., Bless, R. C., & Hanbury Brown, R. 1976, *ApJ*, 203, 417
- Cunto, W., Mendoza, C., Ochsenbein, F., & Zeippen, C. J. 1993, *A&A*, 275, L5
- Fitzpatrick, E. L., & Massa, D. 1999, *ApJ*, 525, 1011
- Garhart, M. P., Smith, M. A., Levay, K. L., Thompson, R. W. 1997, *International Ultraviolet Explorer New Spectral Image Processing Information Manual, Version 2.0*
- González-Riestra, R., Cassatella, A., & Wamsteker, W. 2001, *A&A*, 373, 730
- Grevesse, N., & Sauval, A. J. 1998, *Space Science Review*, 85, 161
- Gulliver, A. F., Hill, G., & Adelman, S. J. 1994, *ApJ*, 429, L81
- Hauschildt, P. H., Allard, F., & Baron, E. 1999, *ApJ*, 512, 377
- Hayes, D. S. 1985, *Proc. of IAU Symposium No. 111*, 225
- Holweger, H. 1970, *A&A*, 4, 11
- Hubeny, I. 1981, *A&A*, 98, 96
- Hubeny, I., & Lanz, T. 2000, *SYNSPEC A User's Guide, v. 43*
- Ilijić, S., Rosandić, M., Dominis, D., Planinić, M., & Pavlovski, K. 1998, *Contributions of the Astron. Observatory Skalnaté Pleso*, 27, 467
- Kupka, F., Piskunov, N., Ryabchikova, T. A., Stempels, H. C., & Weiss, W. W. 1999, *AASS*, 138, 119
- Kurucz, R. L. 1992, *Rev. Mexicana Astron. Astrofis.*, 23, 181
- Massa, D., & Fitzpatrick, E. L. 2000, *ApJS*, 126, 517 (M&F)
- Moon, T. T., & Dworetzky, M. M. 1985, *MNRAS*, 217, 305
- Mozurkewich, D., Armstrong, J. T., Hindsley, R. B., Quirrenbach, A., Hummel, C. A., Hutter, D. J., Johnston, K. J., Hajian, A. R., Elias, Nicholas M., II, Buscher, D. F., Simon, R. S. 2003, *AJ*, 126, 2502

- Nelder, & Mead 1965, *Computer Journal*, 7, 308
- Pérez Hernández, F., Claret, A., Hernández, M. M., & Michel, E. 1999, *A&A*, 346, 586
- Przybilla, N. 2002, PhD Thesis, Ludwig-Maximilians-Universität München
- Qiu, H. M., Zhao, G., Chen, Y. Q., & Li, Z. W. 2001, *ApJ*, 548, 953
- Snedden, C. 2002, *MOOG An LTE Stellar Line Analysis Program*
- Stürenburg, S., & Holweger, H. 1990, *A&A*, 237, 125
- Terež, È. I. 1982, preprint
- Tull, R. G., MacQueen, P. J., Sneden, C., & Lambert, D. L. 1995, *PASP*, 107, 251
- Vasil'Yev, I. A., Merezhin, V. P., Nalimov, V. N., & Novosyolov, V. A. 1989, *Information Bulletin on Variable Stars*, 3308, 1
- Vernazza, J. E., Avrett, E. H., & Loeser, R. 1976, *ApJS*, 30, 1
- Walgate, R. 1983, *Nature*, 304, 681
- Wedemeyer, S. 2001, *A&A*, 373, 998
- Wilner, D. J., Holman, M. J., Kuchner, M. J., & Ho, P. T. P. 2002, *ApJ*, 569, L115

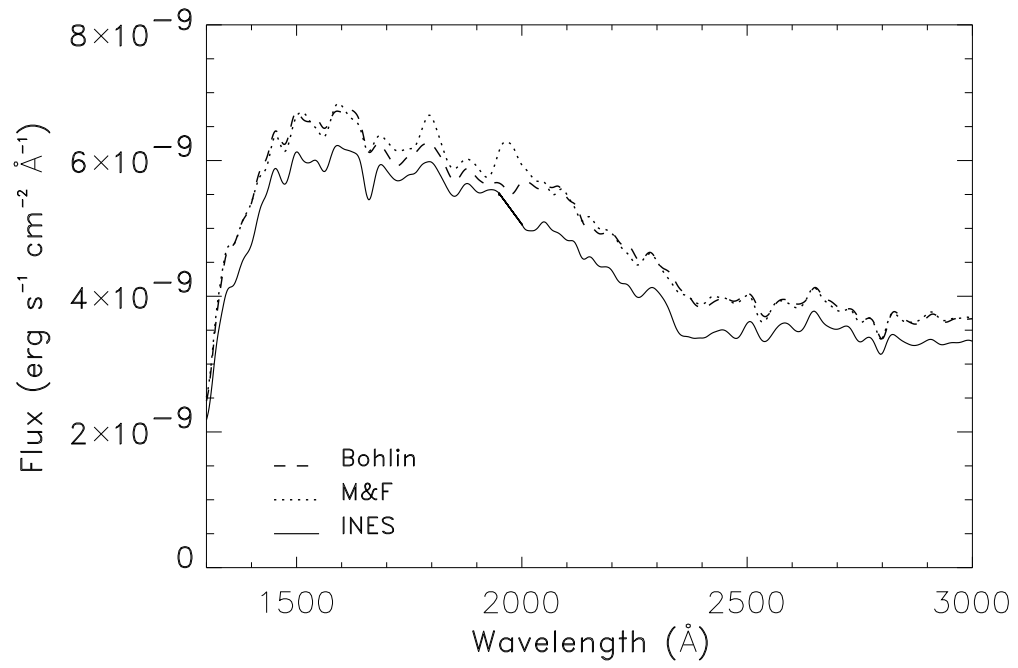


Fig. 1.— Comparison of the observed fluxes in the UV obtained with different calibrations of the IUE satellite smoothed by convolution with a Gaussian profile with FWHM = 25 Å (see text for details).

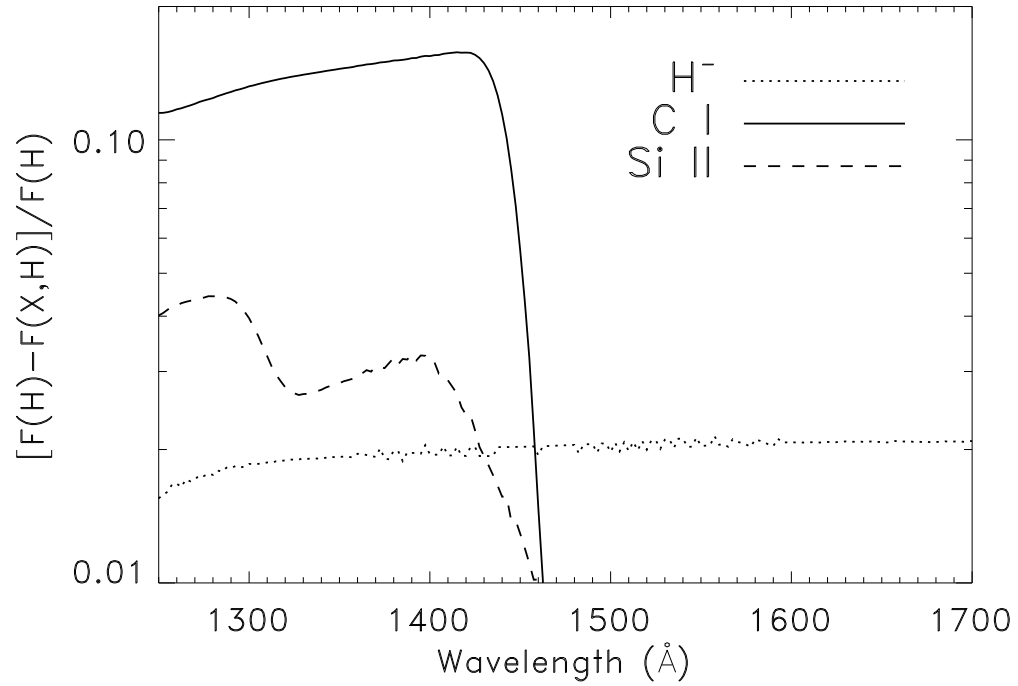


Fig. 2.— Relative difference between the flux computed taking into account neutral H and each ion X explicitly ($F(X,H)$) and the flux obtained by just taking into account neutral H explicitly ($F(H)$). The change in neutral H opacity is also considered in the line labeled as H^- , because the number of protons is constant, and therefore the abundance of neutral H diminishes when including H^- . Note the importance of $C\ I$ below 1450 Å, and that of H^- above this wavelength.

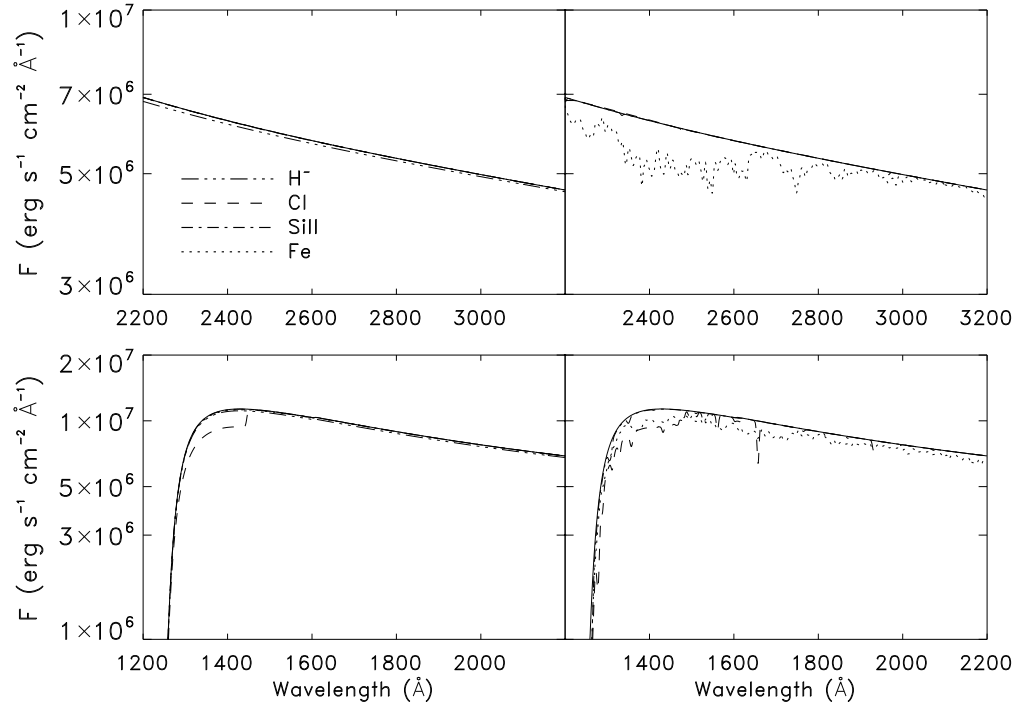


Fig. 3.— *Left*: Emergent flux when only the continuum absorption produced by H^- , Cl , SiII and Fe is considered. *Right*: Emergent flux when the total (continuum+metal line) opacity is considered. The curve corresponding to H^- has been omitted in the right panels for clarity. The solid line is the flux when no opacity is considered.

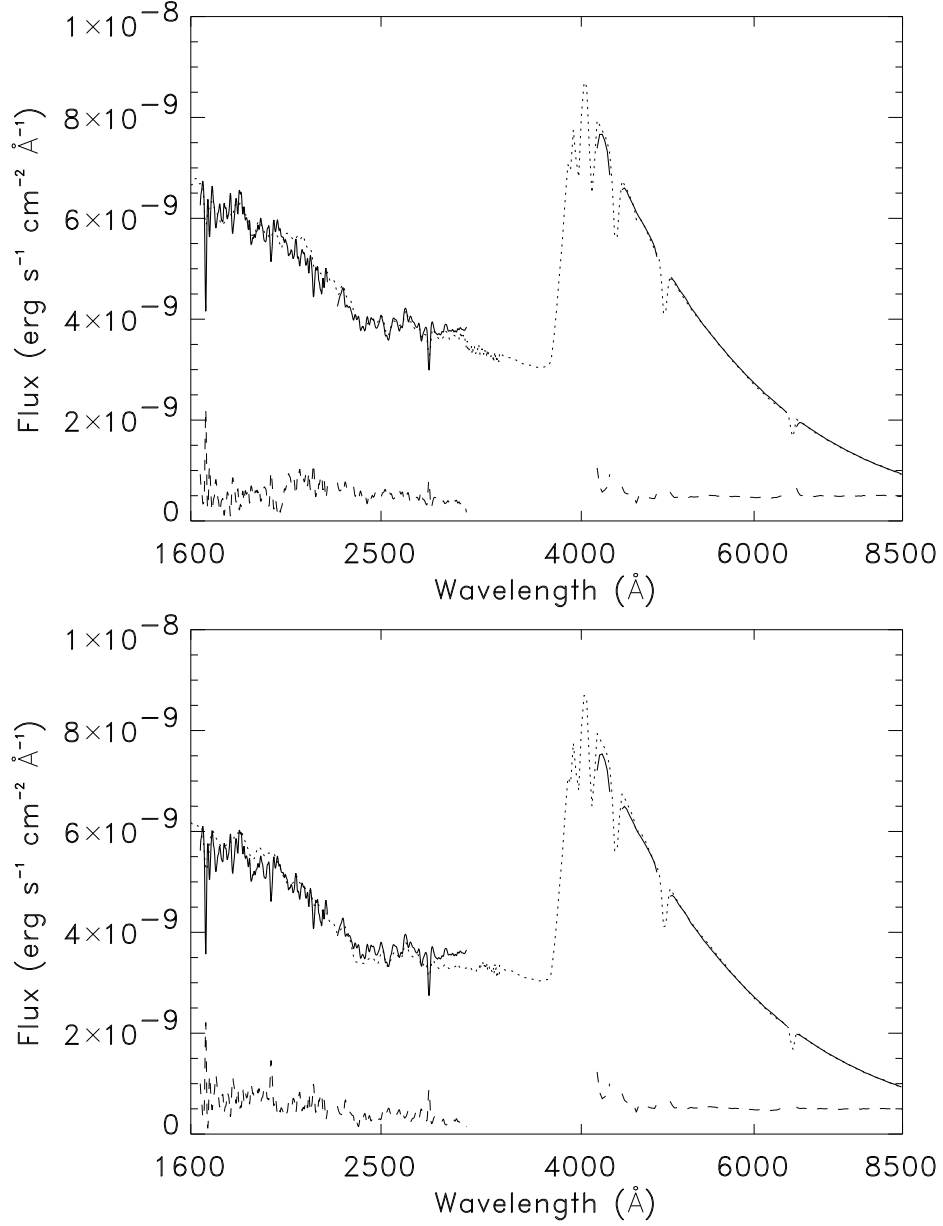


Fig. 4.— Best fit between the observed flux of Vega (dotted line) calibrated by Bohlin (top) and INES (bottom), and the computed flux (solid line). The residuals (observed minus computed flux plus a constant) are also shown (dashed line). The stellar parameters associated with the adopted model atmosphere are shown in Table 2.

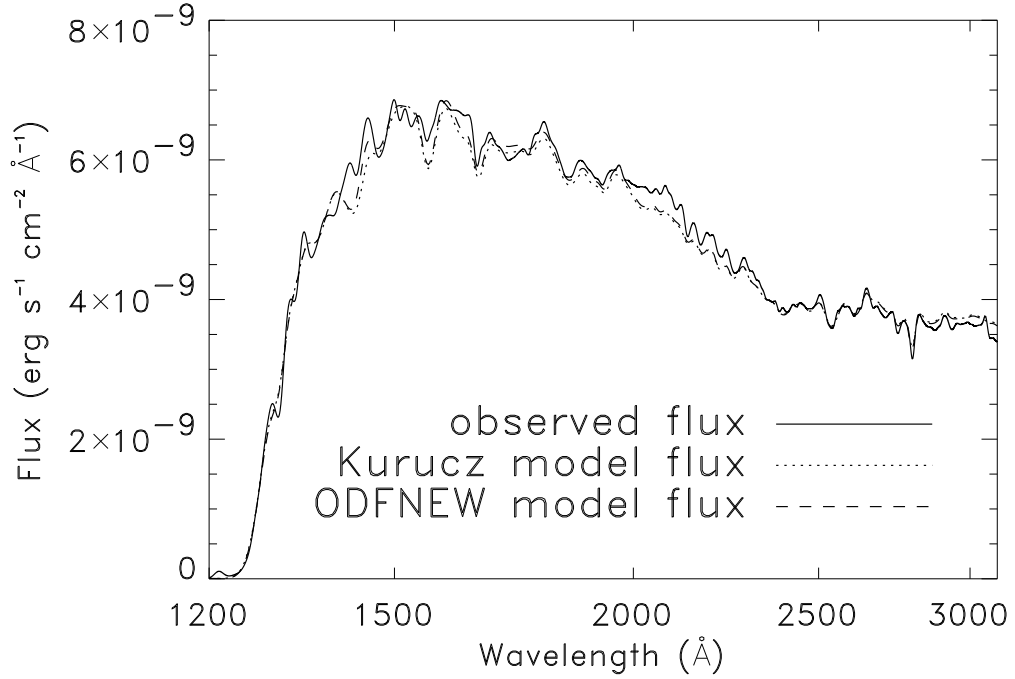


Fig. 5.— Comparison between the observed spectrum of Vega (mean of Bohlin’s and M&F) and the computed spectrum using a Kurucz model atmosphere with the following parameters: $T_{\text{eff}} = 9620$ K, $\log g = 3.98$, $[M/H] = -0.7$, $[Si/H] = -0.90$ and $[C/H] = 0.03$ and the computed spectrum using an ODF model atmosphere with the following parameters: $T_{\text{eff}} = 9575$ K, $\log g = 3.98$, $[M/H] = -0.7$, $[Si/H] = -0.90$ and $[C/H] = 0.03$. The adopted angular diameter is 3.27 mas.

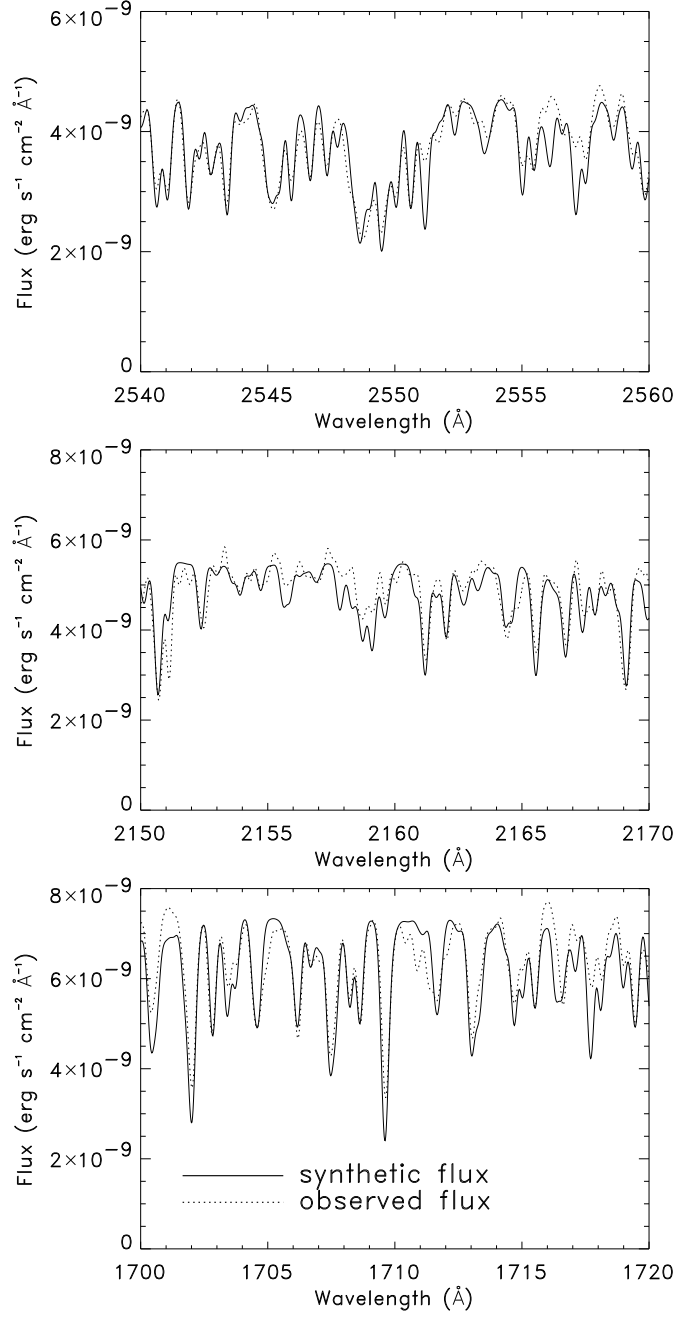


Fig. 6.— Comparison between the observed flux of Vega (dashed line, INES multiplied by 1.1 to take the fluxes to the HST scale) and the computed flux (solid line) at high resolution. The stellar parameters associated with the adopted model atmosphere are $T_{\text{eff}} = 9620$ K and $\log g = 3.98$. The angular diameter used is 3.27 mas.

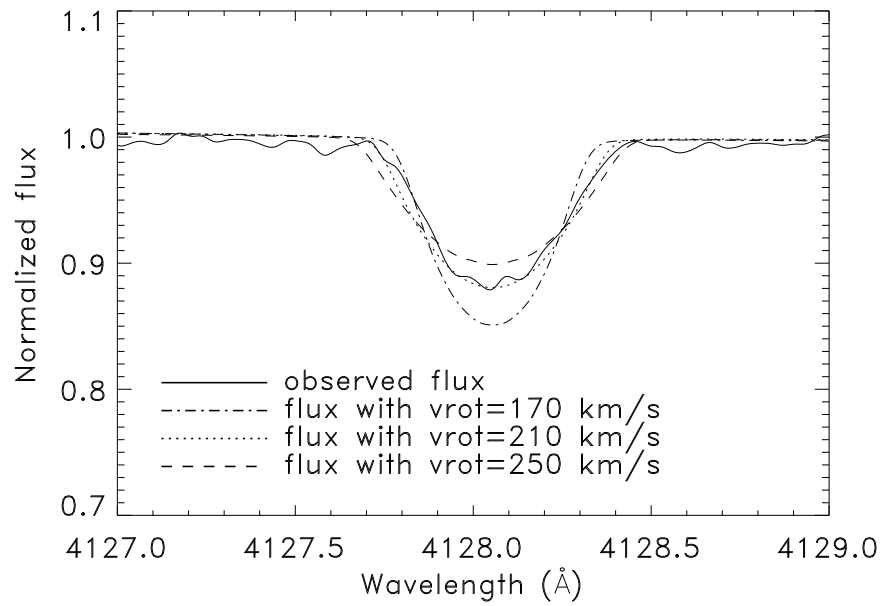


Fig. 7.— Comparison of the normalized high-resolution observed flux next to Si II λ 4128.07 Å and the normalized synthetic fluxes using $T_{\text{polar}}=9595$ K and $i=6$ degrees and different rotational velocities: $v_{\text{rot}}(\text{eq})=170, 210$ and 250 km/s.

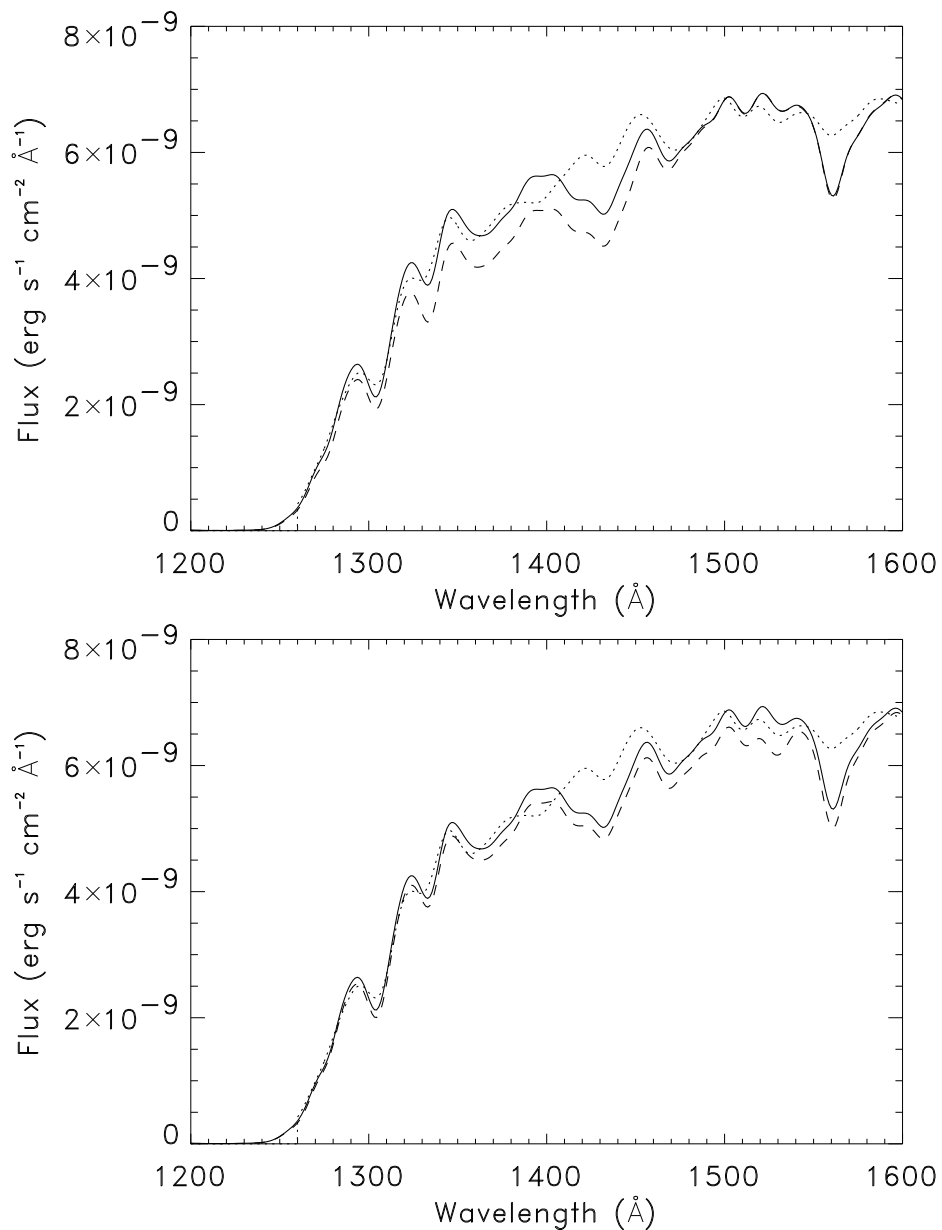


Fig. 8.— Comparison between the observed flux of Vega (dotted line) and the computed flux using $[C/H] = +0.03$ (solid line, top) and $[C/H] = +0.23$ dex (dashed line, top) and the computed flux using $[Si/H] = -0.90$ dex (solid line, bottom) and $[Si/H] = -0.70$ dex (dashed line, bottom). The stellar parameters associated with the adopted model atmosphere are those obtained in Section 3.3.

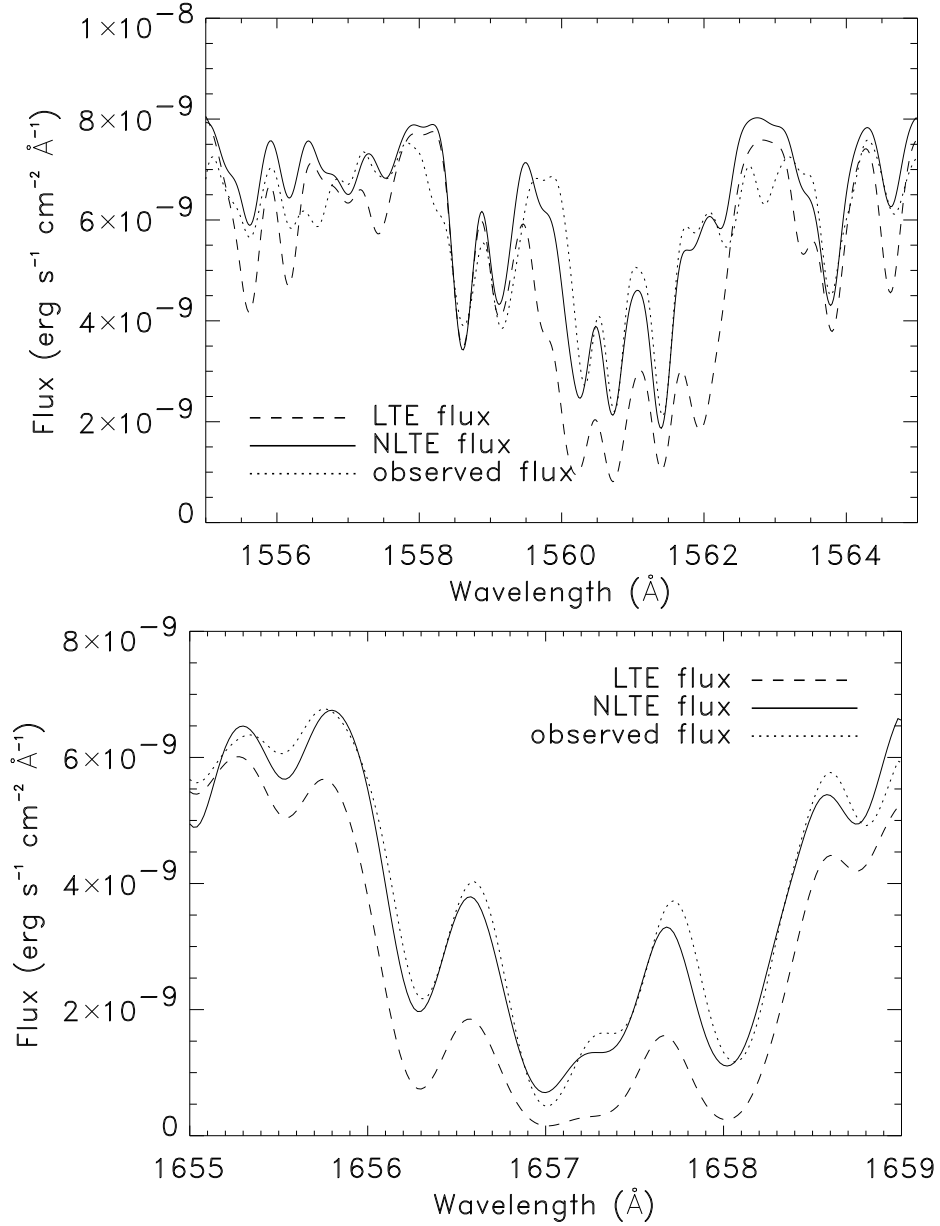


Fig. 9.— Comparisons between the observed spectrum of Vega (mean of Bohlin’s and M&F) and the computed spectrum next to two regions (which have a poor fit in LTE in low resolution) using a Kurucz model atmosphere with the following parameters: $T_{\text{eff}} = 9620$ K, $\log g = 3.98$, $[M/H] = -0.7$, $[\text{Si}/H] = -0.90$ and $[\text{C}/H] = 0.03$, in LTE and in NLTE. The regions are ~ 1560 Å (top) and ~ 1657 Å (bottom). The adopted angular diameter is 3.27 mas.

Table 1. Spectra from different IUE web pages averaged to calculate the calibrated spectrum of Vega with different dispersion and wavelength ranges. M&F fluxes are obtained from the MAST-IUE web page and INES fluxes from the INES web page.

calibration	dispersion	camera name	wavelength range	spectrum numbers
M&F and INES	low	SWP	1150-2000 Å	27024, 29864, 30548, 30549, 32906, 32907
M&F and INES	low	LWP	1850-3300 Å	07010, 07038, 07888, 07889, 07902, 07903, 07904, 10347, 10348
INES	high	SWP	1150-2000 Å	01188, 24504, 32870, 32887, 33633, 38411, 42521, 45285
INES	high	LWR	1850-3300 Å	07585, 08630
INES	high	LWP	1850-3300 Å	07490, 12617, 17648, 21295, 23642

Table 2. Parameters and errors of the best fit between synthetic and observed spectra of Vega using different calibrations.

calibration	T_{eff} (K)	θ (mas)	σ_{1622}	σ_{2230}	σ_{4085}
Bohlin's	9631	3.272	4.9 %	2.9 %	1.3 %
INES	9458	3.324	5.9 %	5.7 %	1.4 %

Table 3. Parameters for Vega according to the literature.

Reference	T_{eff} (K)	θ (mas)	[M/H] (dex)
Code et al. (1976) ¹	9660 ± 140	3.24 ± 0.07	-
Castelli & Kurucz (1994) ²	9550	-	-0.5
Ciardi et al. (2001) ³	9553 ± 111	3.28 ± 0.01	-
Fitzpatrick & Massa (1999) ⁴	9600 ± 10	3.26 ± 0.01	-0.73 ± 0.06
Moon & Dworetzky (1985) ⁵	9430 ± 200	-	-
Alonso, Arribas & Martínez-Roger (1994) ⁶	9610	3.24 ± 0.07	-0.25
Mozurkewich et al. (2003) ⁷	9657 ± 119	3.225 ± 0.032	-
This paper ⁸	9620^{+61}_{-56}	3.27 ± 0.03	-0.7

¹Obtained from angular size measurements and its absolute flux distribution

²Parameters of the Kurucz model producing the synthetic spectrum that best matches the observed one derived from the model to the observed one (in the visible and the UV, with Bohlin’s calibration, and near-IR). A solar abundance of He has been adopted, with no reddening and with a microturbulence of 2 km s^{-1}

³Angular diameter obtained from interferometry at $2.2 \mu\text{m}$

⁴The uncertainties given are 1σ internal errors for the fittings of the synthetic spectrum derived from Kurucz models to the observed one (in the visible, the near-IR, and the near-UV, with the M&F calibration)

⁵Based on $uvby\beta$ photometry, with error estimation from Qiu et al. (2001)

⁶Using the IFM to calibrate the absolute flux of stars with direct measurements of angular size

⁷Angular diameter obtained from optical interferometry

⁸Using Kurucz (1992) model atmospheres

Table 4. Some of the deepest lines in the regions shown in Fig. 9 (~ 1560 and ~ 1657 Å), where a study of the NLTE effect has been carried out.

λ (Å)	ion
1555.660	Si I
1556.161	Si I
1558.541	Fe II
1558.692	Fe II
1559.085	Fe II
1559.706	Si I
1560.309	C I
1560.682	C I
1560.709	C I
1561.340	C I
1561.438	C I
1562.002	Si I
1563.790	Fe II
1564.612	Si I
1656.267	C I
1656.929	C I
1657.008	C I
1657.379	C I
1657.907	C I
1658.121	C I

Table 5. Chemical abundances obtained from spectral lines in the visible region.

ion	λ (Å)	EW (mÅ)	log(N/X) with parameters from Qiu	log(N/X) with parameters from Przybilla	log(N/X) with our parameters
C I	5052.17	33±4	8.37	8.44	8.47
	5380.34	20±3	8.30	8.37	8.39
	6828.12	7±2	8.25	8.32	8.34
	7111.47	17±5	8.35	8.42	8.44
	7113.18	23±2	8.19	8.26	8.28
	7115.17	23±2	8.34	8.41	8.44
	7116.99	21±2	8.28	8.35	8.37
N I	7423.64	20.5±3	8.11	8.12	8.12
	7442.30	34±3	8.08	8.08	8.09
	7468.31	42±4	8.05	8.04	8.05
O I	5329.68 ¹	23±4	8.77	8.77	8.77
	6158.19 ²	57±3	8.81	8.79	8.80
Mg I	4167.27 ³	20±3	7.10	7.19	7.22
	4702.99	30±3	6.96	7.04	7.07
	5183.60 ⁴	122.5±2	7.40	7.31	7.35
	5528.41	28±2	6.92	7.00	7.03
Mg II	4427.99	5±2	6.88	6.87	6.87
	4433.99	12±2	6.97	6.95	6.95
Al II	4663.05	4.5±2	5.81	5.77	5.77
Si II	4128.07	54±4	7.02	6.97	6.96
	4130.89	68±4	6.85	7.04	7.04
	6347.11 ⁵	114±4	7.63	7.49	7.42
	6371.37	80±3	7.30	7.22	7.23
Ca I	4226.73	58±3	5.62	5.71	5.76
Cr I	5206.02	11±2	5.24	5.35	5.39
	5208.42	15±2	5.26	5.37	5.41

¹This is a set of several weak OI lines according to the line list taken from SYNPLLOT. However, Przybilla (2002) seems to take an effective gf with the central wavelength of the table, which is what we have used

²Comparing the computed triplet with the observed "line"

³Using the log gf of Qiu et al. (2001): -0.79 ; using the log gf of Przybilla's PhD Thesis (2002), -1.71 , it is obtained a value 0.92 dex higher

⁴Important NLTE effect

⁵The abundances using damping parameters from VALD are very different, so we have not used this line to derive the abundance of Si

Table 6. Chemical abundances for Fe obtained from spectral lines in the visible region.

ion	λ (Å)	EW (mÅ)	$\log(N/X)$ with parameters from Qiu	$\log(N/X)$ with parameters from Przybilla	$\log(N/X)$ with our parameters
Fe I	4187.04	11±2	6.74	6.84	6.87
	4187.79	16±3	6.92	7.02	7.05
	4202.03	31±3	6.89	6.97	7.01
	4404.75	53.5±3	6.81	6.84	6.88
	4459.12	7±2	7.06	7.16	7.19
	4494.56	8±2	6.99	7.09	7.13
	4736.77	5.5±2	7.04	7.14	7.17
	5324.18	15±2	7.02	7.11	7.14
	5367.47	8±2	6.89	6.98	7.01
	5369.96	12±2	7.02	7.10	7.13
	5383.37	14±2	6.92	7.01	7.04
	5410.91	9±2	7.00	7.09	7.12
	5569.62	5±1	6.94	7.03	7.07
	5572.84	7±2	6.85	6.95	6.98
	5586.76	11±2	6.95	7.05	7.08
5615.64	13±2	6.94	7.03	7.06	
Fe II	4173.47	61±3	7.01	6.94	6.95
	4178.87	59±3	6.93	6.86	6.87
	4233.17	103±4	7.45	7.15	7.17
	4303.17	42.5±5	6.82	6.80	6.81
	4351.76	73±5	6.88	6.74	6.76
	4385.39	48±4	7.06	7.03	7.04
	4491.40	39±3	6.89	6.88	6.89
	4508.29	58±3	7.13	7.07	7.09
	4515.33	50±4	6.78	6.75	6.76
	4522.62	71±5	6.88	6.76	6.77
	4555.88	61.5±4	6.92	6.85	6.86
	4576.33	27±4	6.87	6.88	6.89
	4582.83	20.5±3	6.87	6.88	6.89
	4583.83	93±5	7.18	6.94	6.95
	4620.51	14.5±3	6.80	6.82	6.83
	4629.34	56±3	6.82	6.76	6.77
	4656.97	11±3	7.09	7.12	7.13
	4923.92	118.5±5	7.37	7.06	7.08
	5018.45	128.5±3	7.55	7.24	7.28
	5169.00	134±3	7.31	7.01	7.05
5197.57	54±4	6.81	6.77	6.78	
5234.66	60±5	7.11	7.04	7.05	
5276.00	64±5	6.86	6.78	6.79	
7711.73	12±3	6.70	6.72	6.73	

Table 7. Chemical abundances obtained from spectral lines in the visible compared with those from the literature, from the UV region, and for the Sun.

ion	log N(X) with parameters from Qiu	log N(X) with parameters from Przybilla	log N(X) with our parameters	log N(X) for the Sun from GS98
C I				
mean	8.30±0.07	8.37±0.06	8.39±0.07	
literature	8.46±0.13	8.23±0.11		8.52
UV continuum			8.55 ^{+0.34} _{-0.48}	
N I				
mean	8.08±0.03	8.08±0.04	8.09±0.04	
literature	8.00±0.02	7.69±0.06 (NLTE)		7.92
O I				
mean	8.79±0.03	8.78±0.02	8.78±0.02	
literature	9.01±0.14	8.57±0.05 (NLTE)		8.83
Mg I				
mean	7.10±0.22	7.14±0.14	7.17±0.15	
literature	6.81 (1 line)	7.02±0.06 (NLTE)		7.58
Mg II				
mean	6.92±0.06	6.91±0.06	6.91±0.06	
literature	6.69±0.05	7.02±0.03		7.58
Al II				
mean	5.81 (1 line)	5.77 (1 line)	5.77 (1 line)	
literature	—	5.84 (1 line)		6.47
Si II				
mean	7.06±0.23	7.08±0.13	7.08±0.14	
literature	6.96±0.06	6.94±0.05		7.55
UV continuum			6.65 ^{+0.57} _{-2.10}	
Ca I				
mean	5.62 (1 line)	5.71 (1 line)	5.76 (1 line)	
literature	5.41±0.09	5.67±0.11		6.36
Cr I				
mean	5.25±0.01	5.36±0.01	5.40±0.02	
literature	5.19±0.17 (CrII)	5.12±0.04		5.67
Fe I				
mean	6.94±0.09	7.03±0.10	7.06±0.09	
literature	6.94±0.12	6.96±0.08		7.50
Fe II				
mean	7.00±0.23	6.91±0.15	6.92±0.15	
literature	6.93±0.13	6.97±0.12 (NLTE)		7.50